Journal of Food Engineering 311 (2021) 110710

Contents lists available at ScienceDirect

Journal of Food Engineering

journal homepage: www.elsevier.com/locate/jfoodeng

Combined 0.2 T static magnetic field and 20 kHz, 2 V/cm square wave electric field do not affect supercooling and freezing time of saline solution and meat samples

Sisay M. Abie [a], Daniel Münch [b,c], Bjørg Egelandsdal [d], Frøydis Bjerke [b], Ivar Wergeland [e], Ørjan G. Martinsen [a,f,*]

[a] Department of Physics, University of Oslo, Oslo, Norway
[b] Animalia – Norwegian Meat and Poultry Research Centre, Oslo, Norway
[c] Faculty of Ecology and Natural Resource Management, Norwegian University of Life Sciences, Aas, Norway
[d] Faculty of Chemistry, Biotechnology and Food Science, Norwegian University of Life Sciences, Aas, Norway
[e] Sci-Group AS, Oslo, Norway
[f] Department of Clinical and Biomedical Engineering, Oslo University Hospital, Oslo, Norway

ARTICLE INFO

Keywords:
Electric field
Magnetic field
Freezing
CAS freezing
Saline
Meat

ABSTRACT

Previous studies proposed that electric and magnetic fields can affect the freezing of biological tissues, including meat. Yet, improved freezing through sole magnetic or combined electro-magnetic field exposure is disputed. Also, as previous studies typically tested very small sample dimensions, it is unclear if the reported effects are transferrable to larger product sizes that are relevant to commercial food freezing. Here we aimed at reassessing previous findings by constructing and testing a scaled-up setup for applying electric and magnetic fields during freezing. Importantly, our setup replicates key technical aspects of previous electro-magnetic freezer designs. We modeled and measured the spatial distribution of electric and magnetic fields generated by this setup. We then studied possible effects of field exposure on freezing of two different volumes of saline water and of meat. We tested four different field treatments: sole magnetic and electric field exposure, a combination of both and a control without altered field exposure. We show that the 20 kHz square wave electric field was largely homogenous, while the static 0.2 T magnetic field was not. We found that none of the field treatments altered freezing dynamics of the three tested sample types. Our findings, hence, do not support previous data obtained with similar electro-magnetic field freezer setups. We discuss how our study that uses very distinct field parameters, may inform the general discussion on the effectiveness of electro-magnetic field exposure during food freezing.

1. Introduction

Freezing extends the shelf life of food. Yet, quality defects are an inevitable consequence of ice crystal build-up during the freezing process. To minimize quality deterioration in frozen foods, freezing innovations are being constantly developed, but actual quality improvements are often unclear or even debated. A case in point is the use of electro-magnetic fields in commercial freezers.

Freezing of water is influenced by different external factors. Several studies show that electric and magnetic fields may cause changes in the physicochemical properties of water, in the structural characteristics of water molecules, and in the interaction between these molecules (Chang et al., 2006; Holysz et al., 2007; Cai et al., 2009). Due to its diamagnetic nature, water is affected by magnetic fields. Such fields can increase the energy of hydrogen bonding by weakening the van der Waals bonding force between the water molecules. As a result, the organization of the water molecule lattice may become more ordered and stable, when exposed to external magnetic fields (Chang et al.,2006). Yet, the opposite effect, i.e. weakened hydrogen bonds in magnetized water, has been described as well (Wang et al., 2013). External electric fields, on the other hand, can decrease the free energy due to reorientation of water molecules and formation of more ordered cluster structure (Orlowska et al., 2009). However, it is also plausible that electric fields may break and weaken the water molecules' hydrogen bonds, which can result in a

* Corresponding author. Department of Physics, University of Oslo, Oslo, Norway.
E-mail address: o.g.martinsen@fys.uio.no (Ø.G. Martinsen).

https://doi.org/10.1016/j.jfoodeng.2021.110710
Received 28 July 2020; Received in revised form 20 May 2021; Accepted 6 June 2021
Available online 8 June 2021

less ordered molecular matrix. The latter effect seems opposite to those caused by the magnetic field (Chang et al., 2006). Overall, findings and theoretical considerations on possible field effects on the lattice of water molecules are inconclusive. Yet, however the specific effects are, electric and magnetic fields have the potential to alter the molecular matrix of water. Building on this, novel freezing technologies have been suggested that make use of electric fields, magnetic fields, and a combination of both.

Several experimental studies have reported effects of such field treatments on freezing. Tang et al. (2019) studied the effect of both, static (SMF) and alternating (AMF) magnetic fields up to 16 mT on the freezing parameters of pork and found that the fields had a significant effect on several of the parameters. The SMF influenced the nucleation point, phase transition time and supercooling time, while the AMF changed the freezing time and phase transition time. Lin et al. (2015) observed a higher survival rate of cells after freezing in the presence of a 0.8 T magnetic field. Kaku et al. (2010) tested a CAS freezer ("Cells Alive System", ABI Corporation Ltd., Japan), which generated a very weak oscillating magnetic field during freezing of individual cells and tissues, which were suspended in a cryoprotectant (10% dimethyl sulfoxide). According to the report, superior cell viability and tissue integrity was observed compared to controls that were cryopreserved without artificial magnetic field exposure (Abedini et al., 2011). Lin et al. (2013) also found a higher cell survival rate and increased cell membrane rigidity after freezing in SMFs of 0.4 T compared to 0.2 T. In a more recent study (Dalvi-Isfahan et al., 2016), a noticeable impact of SMF exposure on the nucleation temperature was reported, as well as a 60% reduction of ice crystal size with a static electric field (SEF) of 580 V/cm. Finally, a significant effect of combined SMF and square wave electric field (SqWEF) exposure during freezing of saline solutions (2 mL) was reported for different freezing parameters, including phase transition time, supercooling and ice crystal size (Mok et al., 2015). Specifically, the authors report that combining a SqWEF (20 kHz, 1.78 V/cm) with a repulsive SMF (estimated flux density of 50 mT) "resulted in an effective and synergistic freezing process, forming uniformly round and the smallest mean size of ice crystals in the shortest phase transition". While no statistical analyses on possible effects on phase transition time were provided for that specific experiment, the authors report, e.g., a 54.7% shortening of the phase transition time for SqWEF only exposure, and a 30.4% shortening compared to the control, when SqWEF and repulsive SMF were combined.

Woo et al. (2010) suggested that electric and magnetic fields could control spontaneous nucleation or produce unclustered uniform ice crystals, which may provide an advantage in preserving frozen food and biological products. Jin et al. (2020) used SMFs up to 18 mT and found increased nucleation time and decreased phase transition time for 0.9% NaCl solutions. However, Otero et al. (2018) found no effect on the supercooling and freezing kinetics of 10 ml pure water and 0.9% salt solution using a SMF (field strength of 0–359 mT). Furthermore, theory and experimental data on the possible effect of combined electric and magnetic field are non-conclusive (Otero et al., 2016). We argue that the lack in reproducibility may be linked to a lack of standardization in published experimental designs – in agreement with (Otero et al., 2018). Therefore, simple setups that are easy to manufacture and control are needed to thoroughly probe hypotheses and conflicting findings published in the recent years.

In this paper, we have developed a scaled-up setup for highly controlled electric and magnetic field assisted freezing in order to investigate possible effects on different sample dimensions. This enabled us to re-assess previously documented effects on saline samples (Mok et al. (2015)). We also tested for possible effects on an actual food sample (pork), as the CAS technology was suggested to improve food freezing. We used finite element modeling to model the electric and magnetic fields inside the field box. We then tested if direct measurements of spatial field distribution can confirm the modeled data for our field box design. Finally, freezing studies with three sample types were conducted as proof-of-principle tests.

2. Materials and methods

2.1. The box and magnet holder

The field box was built from aluminum, acrylic glass and mica materials, which all have magnetic permeability close to that of free space. The overall dimensions of the box were 40 cm × 30 cm × 20 cm including three different compartments (Fig. 1). These were two drawers (40 cm × 30 cm × 5 cm) at the top and bottom, which housed the magnets. The treatment chamber (40 cm × 30 cm × 10 cm) between the two drawers allowed to expose multiple samples to SqWEF and SMF.

In addition to the bigger box there were two similar boxes of 30 cm × 20 cm × 2.55 cm (Fig. 1B), which were used for assembling and packing the magnets that subsequently were placed in the drawer boxes. These were made from a 2 cm strong plastic frame with a bottom of 15 mm waterproof wood and a 0.6 cm plastic mica sheet as top cover. In the bottom 15 mm wooden panel, we drilled 12 identical 5.1 cm × 5.1 cm x 0.3 cm slots. These were used for attaching a thin metal plate (screwed to the bottom panel) that kept the magnets in place. Such support was necessary to hold the magnets affixed, despite the strong forces that adjacent magnets exert on one another.

The field box was housed in a commercial chest freezer (TM 400 Frigor, Vibocold A/S, Denmark), which was set to a temperature of −26 ± 2 °C. The internal dimensions of the freezing chamber were 116 cm × 60 cm × 85 cm (width × depth × height). As in previous reference studies, the freezer did not feature strong air-blast or ventilation capabilities (e.g., Mok et al., 2015; Otero et al., 2018). For the controls ('no field exposure'), we used a 'dummy box'. This was essentially built as the field box (see Fig. 1) but lacked the magnetic and electric field generating components.

2.2. The square wave electric field

The generation of a SqWEF requires two devices: a square wave power supply and an electrode pair, which converts the square wave voltage into SqWEFs. A parallel plate capacitor arrangement produces a uniform field between the plates. Two aluminum plates were directly connected to the functional voltage supply. The SqWEF was applied as a square pulse waveform (20 V, 20 kHz), similar to the one described by Cai et al. (2009). We did not observe that the SqWEF interfered with thermocouple measurements, which is corroborated by consistent freezing point values among treatments (raw data not shown).

2.3. The static magnetic field

The static magnetic field is characterized by constant direction and strength, but it is non-homogenous. We produced a static magnetic field in this field box by assembling 24 NdFeB block permanent magnets (each having a surface field of 0.42 T). Each block magnet had a dimension of 5.08 cm × 5.08 cm × 2.54 cm. Permanent magnets were preferred to coils because of their ability to produce much higher magnetic flux densities. The forces between these ultra-strong magnets made it impossible to stack them tightly side by side and a spacing of 2.0–2.5 cm was necessary in order to avoid damage to personnel or material while assembling the box. Measurements of the SMF strength were done with a Hirst Magnetics GM08 Gauss Meter to verify the results of the numerical simulations presented in section 4.2.

One may ask if the magnetic field can influence the electric field, but since the static magnetic field is time-invariant, there will be no change in the magnetic flux with time and hence no induced electric field.

2.4. Assessment of freezing dynamics using saline water and meat samples

To test if SqWEF and SMF exposure can affect freezing curves in real

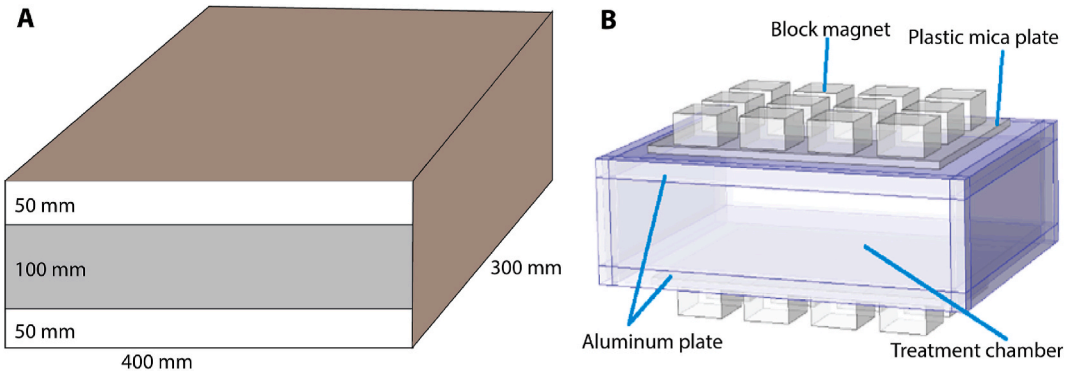

Fig. 1. A. Schematic drawing showing the dimensions of the field box and its parts. The essential elements for generating SMF and SqWEF (compare 1B) were housed in drawers (white) above and below the treatment chamber (grey). **B.** Schematic illustration showing the spatial arrangement of the individual magnets within the drawers of the field box casing and their location with respect to the SqWEF generating aluminium plates, which were connected to a voltage supply.

samples, we used a saline solution as a model system for which composition and volume is highly controllable and data can be more readily compared to previous studies (e.g., Mok et al., 2015; Otero et al., 2018). For a proof-of-principle test we used pork samples as a reference system for meaty foods.

Within the treatment chamber, samples were placed a few millimeters above the surface of the bottom aluminum electrode plate. Three samples were placed in one row that aligned with the center of the three magnets per upper and lower row (compare Fig. 1A). Along this center line, however, samples were placed between two magnets, i.e. halfway between the center points of two adjacent magnets. Three saline samples (replicate: sample) were used in each test (replicate: test run). Tests were repeated for four different conditions (electric field, magnetic field, both fields, and no fields) and for two different volumes of solution. Hence each treatment was represented by twelve replicate samples (three samples x four replicate runs). Meat samples had a similar vertical and horizontal placement in relation to the magnets in one row. Yet, here we tested twelve samples – arranged in three rows – per test run replicate. As with saline, each field condition test was represented by four test run replicates with a total of N = 48 samples for each field treatment.

For testing different volumes of 0.9% NaCl saline solutions we used 2 types of plastic tubes: Nunc cryotubes (13 mm diameter, 50 mm length, NUNC.INS, Denmark) for a sample volume of 2 mL and standard liquid scintillation vials with polypropylene screw caps (28 mm diameter, 60 mm length) for a sample volume of 10 mL. For generating meat samples, we used minced pork meat that was obtained from Animalia's meat processing pilot plant in Oslo (Norway). To achieve a similar cylindrical shape for all samples minced meat was pressed into plastic cylinders (EZ-DripLoss system as described in (Rasmussen and Andersson, 1996)), and samples were finally adjusted to a weight of 10 ± 0.1g.

Saline and meat samples were subjected to four different field settings: a SqWEF (E, 2 V/cm, square wave 20 kHz), a SMF (M, 0.20 ± 0.06 T at the location of the samples), a combination of both fields (EM), and a standard freezing control in the dummy box but without applying external electric or magnetic fields (C). To detect if these treatments could induce changes in the freezing curve, we assessed commonly used parameters to describe freezing characteristics, phase transition time and degree of supercooling (Fig. 2; Mok et al., 2015).

Temperature was monitored with a calibrated Lutron TM-947SD four-channel thermometer (Lutron Electronic, Taiwan) with attached thermocouple probes (Fluke sure grid 80PK-1 beaded, type k). Plastic rings were attached to the wires of the thermocouple probes to fixate sensors at the center of each sample. A temperature sampling rate of 1 Hz was chosen to sufficiently represent rapid changes, such as the temperature increase following initial nucleation, i.e. supercooling (Fig. 2A).

For tests with saline solutions, we determined phase transition time (PTT) and the degree of supercooling (SCC) as described by Mok et al. (2015) and shown in Fig. 2A. Briefly, the temperature and time point, where freezing (nucleation) begins, also defines the starting point of phase transition, and is readily obtainable based on calculating the freezing point depression for a certain saline concentration. For smaller saline volumes, a sharp temperature rise after supercooling typically precedes freezing, making the freezing point a highly accessible and

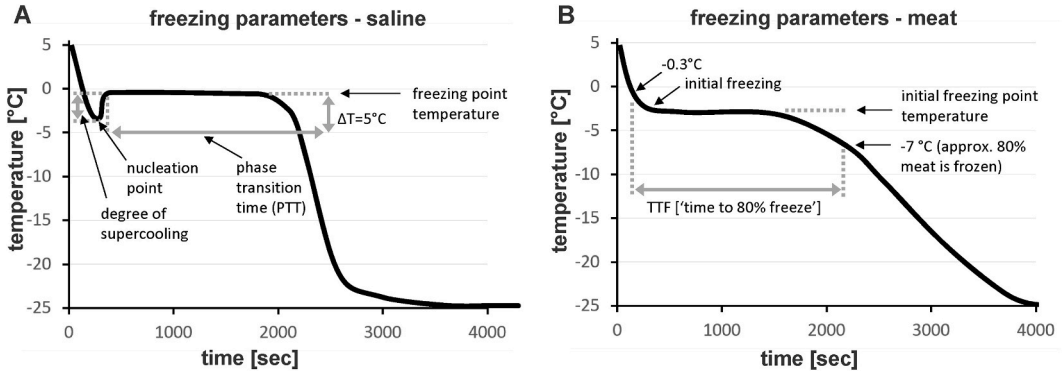

Fig. 2. A. Freezing profile and parameters analyzed in saline water. The degree of supercooling is defined as the temperature difference between the freezing point and the nucleation point. The time difference between the nucleation point and the point where the temperature drops by 5 °C from the freezing point temperature is defined as the phase transition time (Mok et al., 2015). **B.** Freezing profile and parameters analyzed in meat. Phase transition stages are less defined in meat, with typically no detectable supercooling (compare 4.3). As an alternative for PTT values **(A)**, we therefore calculated the time needed for meat to traverse a temperature range from −0.3 °C to −7 °C (TTF). The upper limit (−0.3 °C) is a temperature threshold just above the initial freezing point of all meat samples. At −7 °C approximately 80% of meat is frozen, according to (Sanz et al., 1999).

robust parameter to extract for such sample types (compare, e.g., Figs. 1A and 6A; for data on super cooling, see also results section). Obtaining comparable data on freezing point temperature and the corresponding time point, however, is challenging for complex materials, such as food samples. Firstly, supercooling – i.e., a lowering of the temperature below the freezing point and without ice nucleation – is a highly stochastic event. Such supercooling is readily induced in small volumes of relatively homogenous aqueous solutions. The probability of random ice crystal nucleation increases within larger samples and in samples with more complex material blends. Supercooling effects, therefore, can be less pronounced or become undetectable in meaty food products (compare Wilson et al., 2003 and chapter 4.3 in the results section; compare Fig. 1A and B as well as Figs. 6A and 7B). Secondly, phase transition time in meat is typically given as the time it takes for meat to traverse a fixed temperature range: from initial freezing to a time point, when for example 80% of the meat's water fraction is frozen (e.g., [-1.1 °C to −7 °C] in Sanz et al., 1999 and Bevilacqua et al., 1979). However, in contrast to defined saline solutions, definitions and temperature ranges for the initial freezing point in meat differ among published reports and can be as low as −10 °C (e.g., Bøgh-Sørensen, 2006). Further complicating this, phase transition events are necessarily less defined in meat as compared to more simple material blends, such as saline, as the freezing point is not uniform in meat and among its different components, such as extra and intra-cellular electrolyte solutions with varying amounts of soluble macromolecules. Consequently, the temperature curves for meat become rather 'flat', when approaching the freezing point. Hence, extracting the time point, when freezing (nucleation) starts, is more challenging for meat as compared to saline (compare Fig. 2A and B and 6A and 7A). Reliable data extraction in practice is further complicated by inevitable, small temperature bias, e.g., from biological sample- and temperature logger-variation. This can generate a large variation in extracted time parameters, when using a fixed temperature close to the estimated freezing point in real freezing curves, i.e. when the temperature curve flattens out. As a more reliable parameter to define the phase transition time and its starting point, we therefore used a temperature value just above the estimated initial freezing point, where the temperature slope is still steep, and small differences in measured temperatures have less effect on reading out a time point close to initial freezing (−0.3 °C; compare Fig. 2B). Phase transition in meat ('time to freeze', TTF) was hence defined as the time passed between temperature values of −0.3 °C to −7 °C.

To assess overall effects of field treatments on freezing parameters for saline, we calculated General Linear Model (GLM) statistics with treatment and sample volume as fixed factors. GLM modeling allowed for calculating the relative contributions of the fixed factors to the overall variance ('explained variance'). For meat samples, treatment was the only fixed factor. Pairwise comparisons between individual treatments and the control were carried out by calculating Tukey' statistics. Lastly, inevitable differences in the temperature response among loggers may introduce bias that could mask possible effects. To address this, we have also calculated GLM statistics with logger identity as a random variable.

3. Theory and calculation

Simulation was performed in order to show and verify the spatial distribution of field strength. This was done for both, the square wave electric field and the static magnetic field using the AC/DC Module of COMSOL Multiphysics ver. 5.2 (Stockholm, Sweden). This software employs the finite element method (FEM), a numerical technique in mathematics for calculating approximate solutions of partial differential equations (PDEs) with known boundary conditions (Reddy, 2005). With this method, the partial differential form of Maxwell's equations of electromagnetic phenomena can be solved numerically.

3.1. Numerical modeling of the square wave electric field

We developed and validated a model describing the SqWEF distributions inside the box. Such distributions are difficult to determine experimentally.

3.1.1. Geometry and governing equations

The geometry of the freezing box model is shown in Fig. 1. The box consisted of two parallel aluminum plates with a 40 cm × 30 cm area separated by 10 cm and connected to a power supply. The gap between the two plates is filled with air of relative permittivity $\varepsilon_r = 1$ and with conductivity $\sigma = 0$. The surrounding space was also modeled to account for the fringing fields (non-uniform fields at and outside the border of the volume defined by the two plates). This problem was discretized with the FEM using triangular grid elements (mesh). Moreover, to accurately model the field, the AC/DC module describing electrostatic as well as electrodynamic effects was selected. The governing equations are adapted from COMSOL Multiphysics by selecting the electrostatics interface from the AC/DC module. The AC/DC Electrostatics module is governed by charge conservation,

$$\vec{\nabla} \cdot \boldsymbol{J} = 0 \tag{1}$$

where $\boldsymbol{J}$ is the current density, and $\rightarrow_\nabla$ is a vector differential operator.

And from classical electrostatics,

$$\vec{\nabla} \cdot \boldsymbol{D} = \rho_f \tag{2}$$

$$\boldsymbol{E} = -\vec{\nabla}\cdot\phi \tag{3}$$

where $\boldsymbol{E}$ is the electric field, ϕ is the electric potential, $\boldsymbol{D}$ is the electric displacement field, and ρ_f is the free electric charge density.

3.1.2. Boundary conditions

To solve the above differential equations, the boundary conditions had to be defined for every application. The conductive media application mode applies only to the capacitor part of the model. For inlet, outlet and insulator (air) gap, electric isolation was assumed:

$$\boldsymbol{n} \cdot \boldsymbol{D} = 0 \tag{4}$$

The electric potential ϕ is defined at the upper electrode plate with

$$\phi = \phi_0 \tag{5}$$

where ϕ_0 is the maximum potential of the pulse.

The other electrode was grounded, i.e. the potential was zero.

3.2. Numerical modeling of the static magnetic field

We then aimed to simulate the spatial distribution features of the magnetic field, which is induced by permanent magnets and, hence, is largely temperature-independent within the narrow temperature range, where tissue freezing occurs.

3.2.1. Geometry and governing equations

Each set contained 12 pieces of block permanent magnets arranged in parallel (the same magnetization direction) to each other. These 12 blocks of magnets were assembled and packed in 30× 20 × 2.55 cm^3 sized boxes. In this small package the magnets were arranged in 4 columns and 3 rows. The columns and rows were separated by 2.5 cm and 2 cm, respectively.

For a given domain, the magnetostatic field is governed by the following Maxwell equations:

$$\vec{\nabla} \times \boldsymbol{B} = 0 \tag{6}$$

$$\vec{\nabla} \times \boldsymbol{H} = \boldsymbol{J} \tag{7}$$

where **B** and **H** are magnetic flux density and magnetic field intensity, respectively, which are related by the constitutive equation $\boldsymbol{B} = \mu \boldsymbol{H}$, where μ is the permeability of the materials. In the presence of a permanent magnetization $\boldsymbol{B}_r$ in the magnetic material (permanent magnet) the constitutive law is:

$$\boldsymbol{B} = \mu \boldsymbol{H} + \boldsymbol{B}_r \tag{8}$$

Using this equation and Maxwell's equation for magnetostatics, we can derive an equation for the scalar magnetic potentials V_m.

$$\boldsymbol{H} = -\vec{\nabla} \cdot V_m \tag{9}$$

$$\vec{\nabla} \cdot (\mu_0 \mu_r \boldsymbol{H} + \boldsymbol{B}_r) = 0 \tag{10}$$

The model uses these equations by selecting the "Magnetic Fields, No Currents" interface from the AC/DC Module.

3.2.2. Boundary conditions

The surrounding volume of the magnets was air. The boundary of the air domain served as the boundary of the system, which means that the exterior plane of the domain served as the boundary to the geometry. The magnetic fields are tangential to the boundary, which is described by the magnetic installation conditions,

$$\boldsymbol{n} \cdot \boldsymbol{B} = 0 \tag{11}$$

The magnetic field is perpendicular to the boundary. This condition is represented by a constant magnetic scalar potential. The model uses the "Zero Magnetic Scalar Potential" condition. If the air box is sufficiently large, the boundary condition used on its remaining exterior boundaries have little influence on the field in the vicinity of the magnets. Although an infinite element domain would give the best results, this model uses the magnetic insulation condition for convenience.

4. Results

4.1. Simulation of electric fields

A full 3D Multiphysics model was set up to study the electric field inside the field box. The SqWEF distribution and strength were simulated, and the results are shown in Fig. 3. Our simulations demonstrate that the electric field distribution was uniform in the treatment chamber of the box and sharply dropped outside the box. Due to the finite size of the capacitor, the field had a maximum at the edge of the plates (fringing fields, compare Fig. 3). However, due to the large volume in the center, the electric field in the treatment zone was homogenous.

4.2. Simulation of magnetic fields

A 3D numerical model was developed to investigate the magnetic field distribution inside the field box due to the arrangement of the block permanent magnets (Fig. 4).

In the absence of moving charges and with permanent magnets, the magnetic field is conservative. An essential property of the magnetic flux density is the formation of complete closed loops around the magnet (Fig. 4). The three-dimensional distribution of the loops is a function of the number, position and magnetic orientation of the magnets.

The magnet system configuration is a combination of both, attraction and repulsion. Unlike attraction of the magnets between the lower and the upper drawers, the repulsive configuration between magnets in the same drawers makes the lines turn horizontally and the field lines simply form a loop around the magnet. This gives rise to the X, Y and Z components of the magnetic field. Such heterogeneity was confirmed by actual field-strength measurements, showing highest values just above the surface of the magnet and lowest values between two neighboring block magnets. Measurement and numerical modeling data are shown in Fig. 5 and show that actual measurements largely confirm the modeled results. Magnetic flux density within the box ranged from approximately 0.02 to 0.45 T (Fig. 5) and made exact sample positioning within the field box essential. To ensure similar field exposure for all replicate

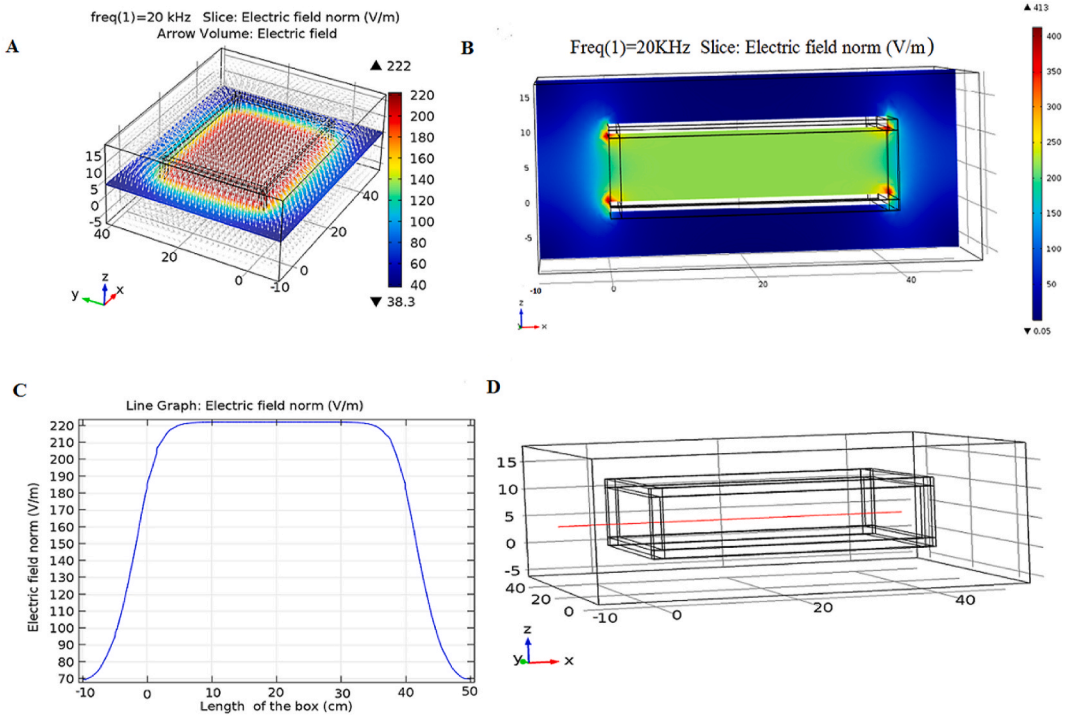

Fig. 3. A. Distribution of electric field across the middle of the parallel plate capacitor system. **B.** Electric field along the vertical slice. **C.** Electric field along the red line in panel (**D**). (For interpretation of the references to colour in this figure legend, the reader is referred to the Web version of this article.)

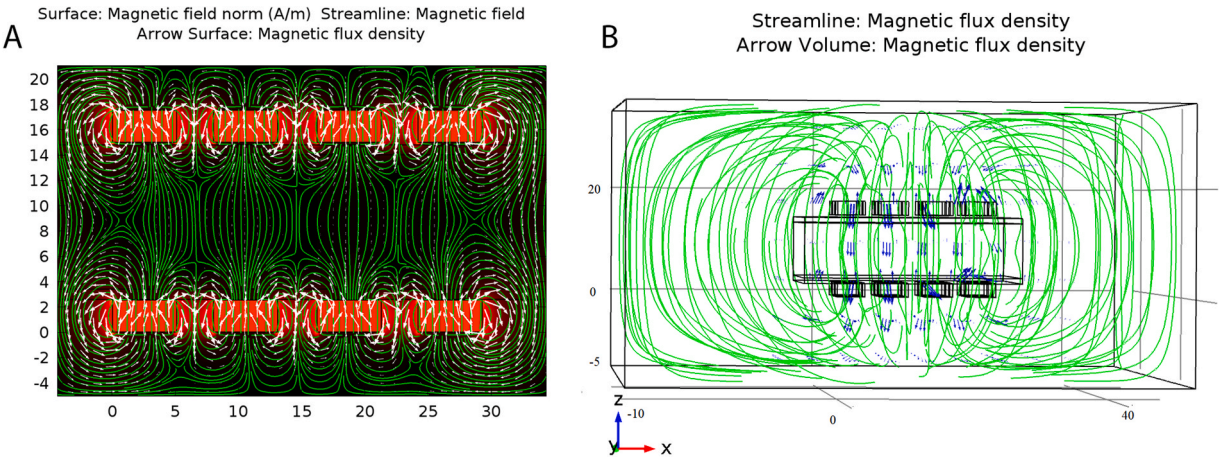

Fig. 4. A. The magnetic field norm as seen from the long side of box. B. Magnetic flux density as seen from the same angle as in **(A)**.

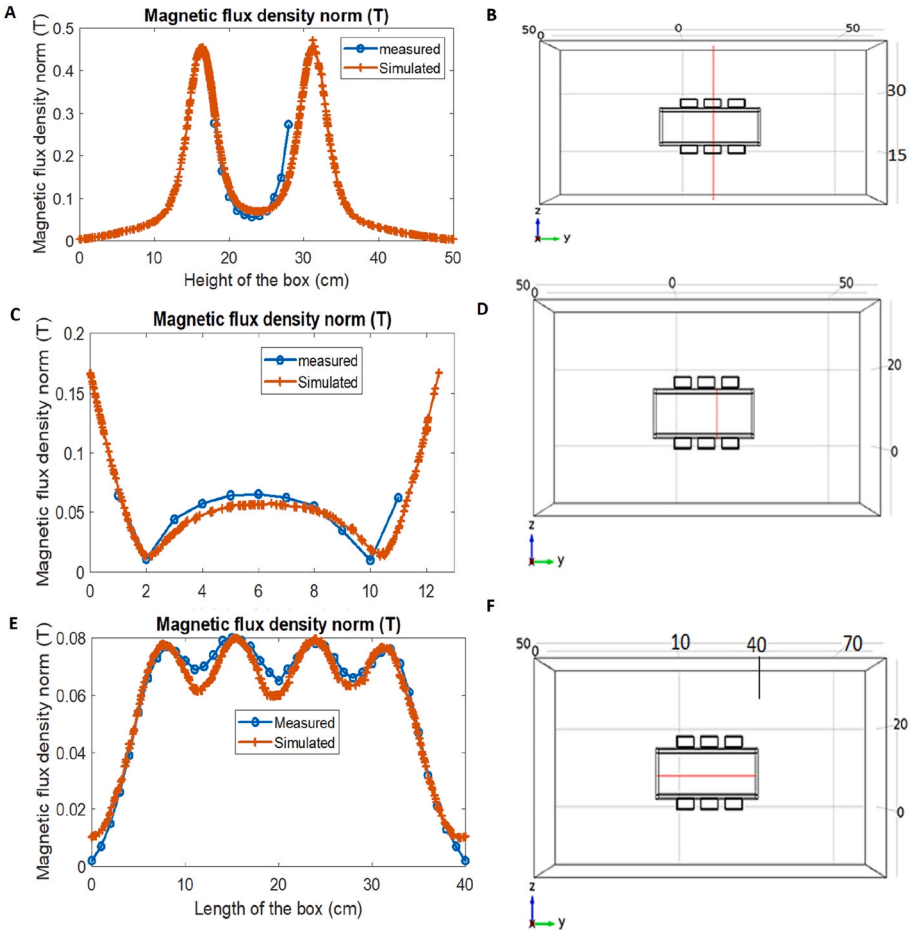

Fig. 5. A. Magnetic flux density along the red line (**B**) - the line passes through the center of one magnet from each side. **C.** Magnetic flux density along the red line (**D**) - the line passes between two magnets. **E.** Magnitude of the magnetic flux density along the mid gap between the upper and lower sets of magnets (which is the center of the field box (**F**)). (For interpretation of the references to colour in this figure legend, the reader is referred to the Web version of this article.)

samples we used a placing matrix with a maximum of 3 × 4 sample positions and holders to keep all samples vertically aligned. For all positions, similar magnetic field exposure was corroborated by simulation data (section 4.2) and direct measurements. Also, since there was ample distance between the samples, there was no reason to believe that individual sample location would have any significant influence on the experimental results.

4.3. Assessing potential field effects on saline solutions and meat samples

To examine previously suggested effects of electro-magnetic fields on freezing profiles, we used a set of three experiments. First, and in line with Mok et al. (2015), we exposed saline samples with a volume of 2 mL to four different field treatments during freezing: electro-magnetic (EM), electric-only (E) and magnetic-only (M) fields, as well as a control (C) without exposure to experimental, external fields (see 2.4). To include

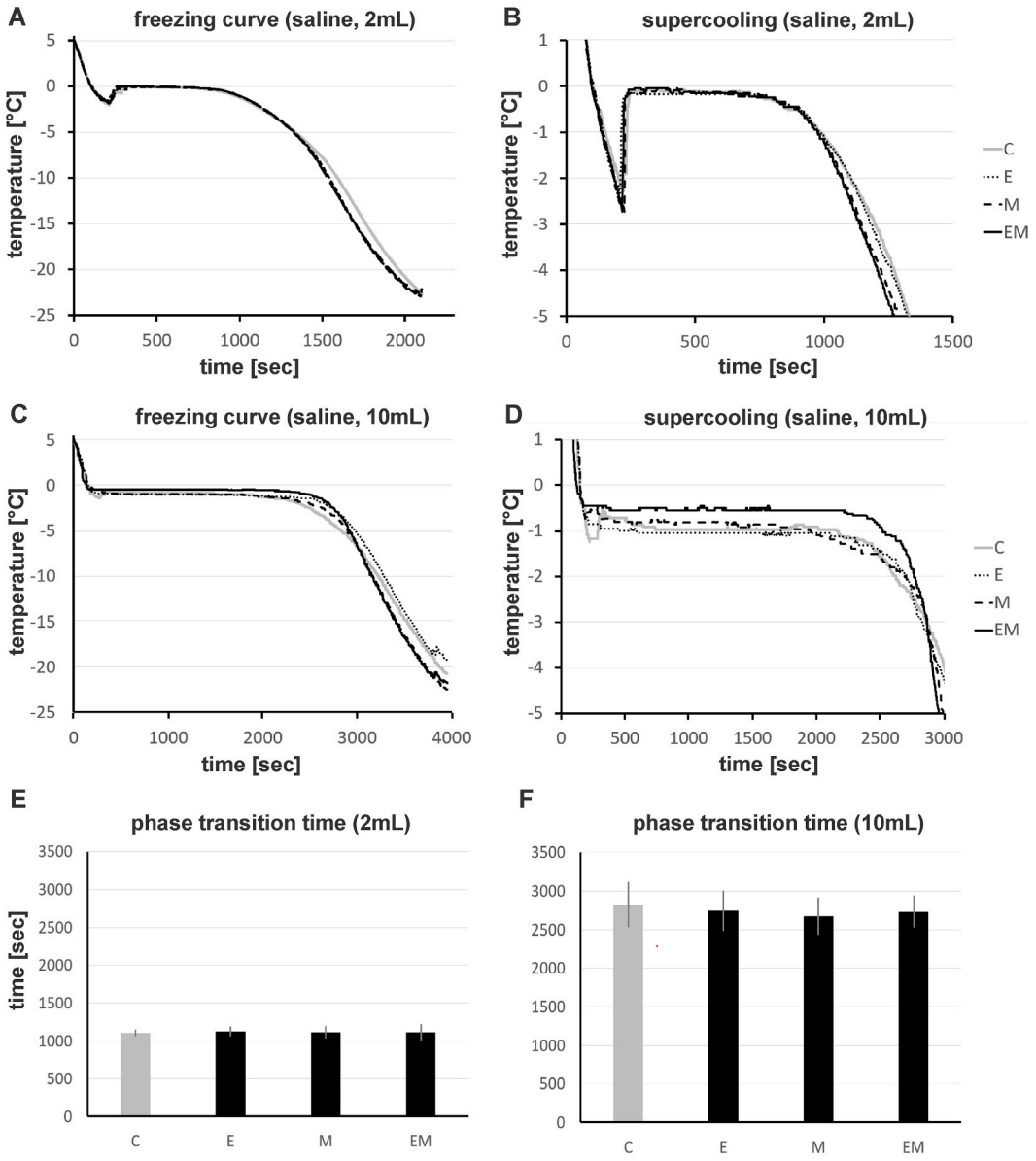

Fig. 6. A. Averaged freezing curves for 2 mL saline solutions exposed to four different field treatments: C = control, E = electrical field, M = magnetic field, EM = combined electric and magnetic fields. **B.** Individual freezing curves showing the period in which supercooling was observed. The graphs show original, not averaged, temperature profiles. Each treatment is represented by the test that showed the median degree of supercooling (SCC). **C.** Averaged freezing curves for 10 mL saline. **D.** Individual freezing curves are shown to reveal potential supercooling (median curve as in **B**). **E, F.** Bar graphs showing the average phase transition ± standard deviation for each treatment and 2 and 10 mL, respectively (N = 12 for each, C, E, M and EM).

samples with more relevance to food applications, we included tests with a larger saline volume of 10 mL and actual pork meat samples of approximately 10 g (10 ± 0,1 g). For all three experiments we assessed "time-to-freeze" parameters (phase transition time, PTT, for saline; 'time to 80% freeze', TTF, for meat; compare 2.4 and Fig. 2). In line with Mok et al. (2015) we also investigated effects of supercooling (degree of supercooling, SCC) for all tested sample types.

Fig. 6 illustrates that our tests did not reveal marked effects of field treatment on PTT and supercooling, neither for 2 mL or 10 mL saline samples. This contrasts with large differences in freezing dynamics between the two different sample sizes.

Using GLM model statistics with field treatment and volume as fixed effects, we found that most of the variation in PTT and in the degree of supercooling was explained by sample volume (explained variance 95 or 85%, respectively) and not by field treatment (0.1 or 1.1%, respectively, see Table 1). In line with this, no significant effect of field treatment on PTT and supercooling was revealed by pairwise comparisons between treatments (Tukey) within each sample size group ([a] for all treatments for both, 2 mL or 10 mL). To test if slight differences among temperature loggers might have masked possible field treatment effects, we have also calculated GLM statistics that included temperature logger identity as a random variable (compare Material and Methods, section 2.7). As before, no overall treatment effects were detected (data not shown).

Adding to the lack of significant field effects, we report that differences in the nominal PTT values among treatments are comparably small: less than 2% and 6% of the total variation, for 2 mL and 10 mL saline, respectively. This suggests, that even if the lack in detecting significant treatment effects may be explained by methodological imperfections, our data still would not support effect sizes that may be relevant to improved freezing applications based on a noticeably shortening of the phase transition time.

Field effects on supercooling were previously suggested as a means

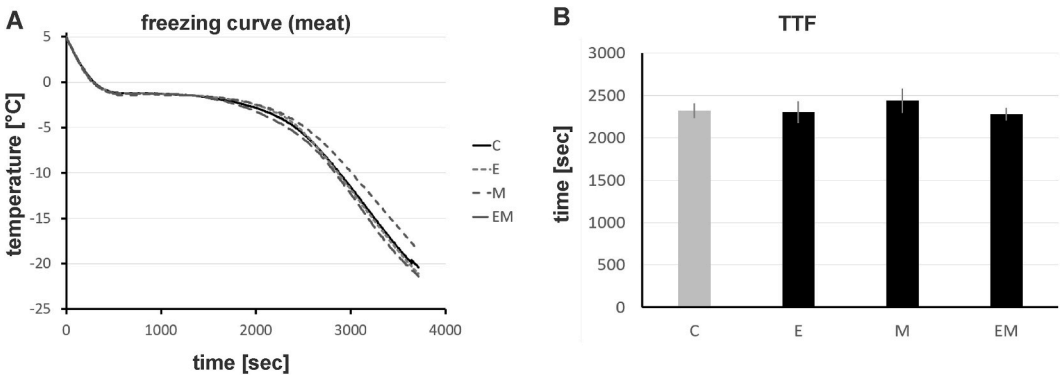

Fig. 7. A. Averaged freezing curves for meat samples exposed to four different field treatments: C = control, E = electrical field, M = magnetic field, EM = combined electric and magnetic fields. **B**. Bar graphs showing a parameter linked to phase transition time in meat (TTF, average ± standard deviation for each treatment, N = 12 for each, C, E, M and EM).

Table 1
Statistics (GLM) for field box tests with two saline volumes (2 mL, 10 mL) and meat samples. P, F and explained variance (EV) statistics are given for a GLM with treatment and volume as fixed effects (saline) or with treatment as the only fixed effect (meat). We tested 48 samples for each of the three sample types and 12 samples per treatment/sample type (** in column N; outliers removed by the GLM statistics are given in brackets). Numbers that have the same letter as superscripts indicate that groups are not significantly different from one another ($P > 0.05$; a for comparisons within rows, x,y for comparisons within columns). Abbreviations: C = control, E = electrical field, M = magnetic field, EM = combined electric and magnetic fields; N = tested sample number for each treatment group, outliers are given in brackets.

Sample	Variable	Vol (mL)	Mean ± SEM				N	Volume	Treatment
			C	E	M	EM			
Saline	Phase transition time (PTT) in s	2	$1107 \pm 13^{a,x}$	$1124 \pm 19^{a,x}$	$1116 \pm 25^{a,x}$	$1113 \pm 32^{a,x}$	48**	$P < 0.001$	$P = 0.642$
		10	$2824 \pm 85^{a,y}$	$2748 \pm 76^{a,y}$	$2678 \pm 70^{a,y}$	$2734 \pm 61^{a,y}$	48**	$F = 1828$	$F = 0.77$
								$EV = 95\%$	$EV = 0.1\%$
Saline	Degree of super-cooling in °C	2	$2.99 \pm 0.07^{a,x}$	$2.73 \pm 0.14^{a,x}$	$2.87 \pm 0.21^{a,x}$	$2.54 \pm 0.22^{a,x}$	48**	$P < 0.001$	$P = 0.019$***
							(-4)	$F = 927$	$F = 3.75$
		10	$0.44 \pm 0.14^{a,y}$	$0.15 \pm 0.01^{a,y}$	$0.09 \pm 0.03^{a,y}$	$0.08 \pm 0.03^{a,y}$	48**	$EV = 85\%$	$EV = 1.1\%$
							(-3)		
Meat, 10 g	Phase transition time (TTF) in s		2321 ± 25^{a}	2326 ± 31^{a}	2445 ± 29^{a}	2280 ± 22^{a}	48**	n. a.	$P = 0.051$
							(-3)		$F = 4.68$
									$EV = 29\%$

for improved freezing (e.g., Mok et al., 2015). As in the latter study, supercooling was typically detected for 2 mL saline samples (Fig. 6B). However, for the larger 10 mL solutions, we found only 2 samples with a degree of supercooling (SCC) > 0.5 °C, and most samples with smaller, but still detectable SCC, were in the control group (Fig. 6D). Together, our data do not support effects of field treatment on supercooling, and also show that supercooling is mostly undetectable for larger sample volumes (10 mL).

Average freezing curves for meat samples with about the same size as the larger saline samples did not show clear differences among field treatments (Fig. 7A). Likewise, no effect of field treatment was revealed by GLM statistics and by pairwise comparisons between individual treatments (Tukey, [a] for all treatments in Table 1).

5. Discussion

We have realized an electro-magnetic field box design that can be reproduced by other research teams and that allowed us to test samples as large as 10 cm^3. With numerical modeling, we have established relevant spatial characteristics of the SqWEF and the SMF within the box and demonstrated a high spatial heterogeneity of magnetic field strength. This was confirmed by measuring the spatial distribution of field strength parameters within the actual field box.

Our tests, with 2 mL saline solutions as well as proof-of-principle tests with larger saline volumes and meat samples, do not lend support to accelerated freezing (phase transition effects) nor to effects that may suppress ice nucleation prior to freezing (super cooling), as previously suggested (Mok et al., 2015). We cannot rule out that optimizing the temperature testing setup or combining the field box with more efficient freezers might improve the detectability of potential field related effects. Yet, even if future studies using our field box design might detect field related effects, our data suggest such effects to be minor (compare Fig. 6A, C and 7A). Further, while our study could not replicate a larger setup with a repulsive SMF orientation, our electric field settings (20 kHz, 2 V/cm) are comparable to Mok et al. (2015), and hence would have suggested a dramatic reduction in phase transition time in our study.

Our findings corroborate earlier skepticism against improved freezing through oscillating and static magnetic fields. Wowk (2012), for example, argued that weak magnetic fields have no or little effect on water freezing, due to water being merely diamagnetic. Specifically, the lack of an intrinsic magnetic dipole moment challenges previous reports on the interaction of water and biological material with weak magnetic fields (e.g., compare Kaku et al., 2010 and Wowk, 2012). A comprehensive review by Otero et al. (2016) provides more fundamental criticism and concludes "[after] examining the information available, it was not possible to discern whether MFs [magnetic fields] have an appreciable effect on supercooling, freezing kinetics, ice crystals, quality, and/or viability of the frozen products." Furthermore, in their recent experimental study the authors also failed to detect effects of SMFs on pure water and saline freezing (Otero et al., 2018). Importantly, while the latter and our study appear to be in conflict with findings by Mok et al. (2015), all three studies used magnetic fields in an approximately 0.1–0.5 T range.

Adding to negligible effects of magnetic fields, our findings highlight another challenge to magnetic freezing that is not yet fully acknowledged, to our knowledge. Most studies, including Otero et al. (2018) and Mok et al. (2015), tested relatively small field designs, often generated

by using two circular magnets. However, solutions relevant for food producers will require up-scaled field box designs with multiple magnets, hence more similar to what we tested. Simulations and actual measurements for the field box design tested here (Fig. 5) clearly demonstrate that magnetic field strength can drop by one order of magnitude towards the center of the freezing chamber – even with a moderate chamber height of 100 mm. Within our box, similar magnetic field conditions were achieved only in an array of relatively small spots, a likely more severe impediment to industrial, larger freezing solutions.

Our conclusions on EMF effects on saline and meat freezing are solely based on parameters related to phase transition time and supercooling. Based on the typical linkage between freezing rate and ice crystal formation (e.g., Leygonie et al., 2012), our data do not lend support to reduced ice crystal formation and freeze damage through EMF freezing. However, we cannot rule out possible changes in ice crystal formation, which were reported previously (e.g., Rohatgi et al., 1974; Mok et al., 2015). Such changes may arise from effects that are not immediately linked to phase transition time. Specifically, several authors found changes in supercooling caused by magnetic fields (e.g., Zhou et al., 2012, reviewed in Otero et al., 2016) and proposed this as a mechanistic route to changed ice nucleation and ice crystal formation. Yet, supercooling and nucleation are inherently stochastic, and supercooling is typically greatly reduced in larger samples as well as in complex material blends, such as biological tissue (Wilson et al., 2003). In line with this, we were unable to identify supercooling in most 10 mL saline samples and in meat samples. We therefore argue that the degree of supercooling is likely not relevant for meat as the muscle matrix is structurally more complex than saline water, with more ice nuclei that are readily formed and with a multitude of chemical compounds that exhibit widely different freezing points.

Our results do not rule out possible effects on freezing through application of stronger magnetic fields that were studied previously (compare, e.g., Inaba et al., 2004; Tagami et al., 1999). Yet generating such fields will hardly be feasible for food processing solutions and may likely pose high workplace hazards. Further, the detection of potential field effects may be contingent of cooling technology, e.g., detectability may improve or decline in slow versus quick freezing setups. However, aiming to reappraise previous claims on magnetic- and electro-magnetic freezing, we used conventional cooling equipment very similar to the relevant reference studies (e.g., Mok et al., 2015).

Likewise, our results do not refute the capacity of electric fields to change freezing rate or ice crystal formation. Electrostatic-assisted freezing is considered to be at an early research state (James et al., 2015 for review). Oscillating electric fields may counteract the formation of large ice crystals by perturbing the orientation of the dipolar water molecules, by causing displacement and vibration (Dalvi-Isfahan et al., 2017). The efficacy of such effects in the context of freezing depends on alternating current (AC) field parameters, including AC frequency (Wei et al., 2006; Sun et al., 2007). In contrast to the static magnetic field, our simulation data (compare Fig. 5) show that the two parallel plates produced a relatively uniform square wave electric field inside the chamber (compare Fig. 3). While the higher spatial uniformity makes the use of oscillating electric fields also suitable for larger samples or food products, ohmic loss will inherently cause the release of thermal energy. Hence heat dissipation is a challenge that likely has prevented wider acceptance of AC-assisted freezing as compared to AC-assisted thawing. However, since the electrodes that generate the electric field in our study were not in direct contact with a sample, most of the electric field will be concentrated in the air gaps and hence the voltage drop across the sample may be very small. In line with this, our calculations show that the dissipated power within the samples was in the lower pico-watt range and consequently should not have contributed to any detectable temperature increase in the samples.

In conclusion, while our data does not lend support for the use of magnetic-field assisted freezing of food products, more studies are needed to establish how AC-assisted freezing can improve freezing and, thus, may reduce freeze damage in food products.

Author contribution

Sisay M. Abie: Conceptualization, Methodology, Software, Validation, Formal analysis, Investigation, Data Curation, Writing - Original Draft, Writing - Review & Editing, Visualization. **Daniel Münch:** Conceptualization, Methodology, Validation, Formal analysis, Investigation, Resources, Data Curation, Writing - Review & Editing, Supervision, Project administration, Funding acquisition. **Bjørg Egelandsdal:** Conceptualization, Methodology, Validation, Formal analysis, Investigation, Resources, Data Curation, Writing - Review & Editing, Supervision, Project administration, Funding acquisition. **Frøydis Bjerke:** Conceptualization, Methodology, Validation, Formal analysis, Investigation, Resources, Data Curation, Writing - Review & Editing, Supervision, Project administration, Funding acquisition. **Ivar Wergeland:** Conceptualization, Methodology, Resources, Supervision, Project administration. **Ørjan G. Martinsen:** Conceptualization, Methodology, Resources, Writing - Review & Editing, Visualization, Supervision, Project administration.

Declaration of competing interest

The authors declare that they do not have any competing interests that are relevant to this research.

Acknowledgements

The authors would like to thank the mechanical workshop at the Department of Physics, University of Oslo, for invaluable help in constructing the field box. We are also indebted to Ole Alvseike and Alexander Mason at Animalia AS and Sanja Krnetic for essential discussions and contributions. Animalia's pilot plant provided meat samples and cutting tools. This work was supported by the MAT-SLF program (Norwegian Agriculture Agency) and the industrial partners Toma Mat AS, Nortura SA, Permanor AS and Sci Group AS (project title: 'Smartfrys', #244441) as well as by the Norwegian Research Council (project title: 'Food Inspector', #294767).

References

Abedini, S., Kaku, M., Kawata, T., Koseki, H., Kojima, S., Sumi, H., Motokawa, M., Fujita, T., Ohtani, J., Ohwada, N., Tanne, K., 2011. Effects of cryopreservation with a newly developed magnetic field programmed freezer on periodontal ligament cells and pulp tissues. Cryobiology 62, 181–187. https://doi.org/10.1016/j.cryobiol.2011.03.001.

Bevilacqua, A., Zaritzky, N.E., Calvelo, A., 1979. Histological measurements of ice in frozen beef. Int. J. Food Sci. Technol. 14 (3), 237–251.

Bogh-Sorensen, L., 2006. Recommendations for the Processing and Handling of Frozen Foods. International Institute of Refrigeration.

Cai, R., Yang, H., He, J., Zhu, W., 2009. The effects of magnetic fields on water molecular hydrogen bonds. J. Mol. Struct. 938, 15–19. https://doi.org/10.1016/j.molstruc.2009.08.037.

Chang, K.-T., Weng, C., 2006. The effect of an external magnetic field on the structure of liquid water using molecular dynamics simulation. J. Appl. Phys. 100, 043917 https://doi.org/10.1063/1.2335971.

Dalvi-Isfahan, M., Hamdami, N., Le-Bail, A., 2016. Effect of freezing under electrostatic field on the quality of lamb meat. Innovat. Food Sci. Emerg. Technol. 37, 68–73. https://doi.org/10.1016/j.ifset.2016.07.028.

Dalvi-Isfahan, M., et al., 2017. Review on the control of ice nucleation by ultrasound waves, electric and magnetic fields. J. Food Eng. 195, 222–234. https://doi.org/10.1016/j.jfoodeng.2016.10.001.

Holysz, L., Szczes, A., Chibowski, E., 2007. Effects of a static magnetic field on water and electrolyte solutions. J. Colloid Interface Sci. 316, 996–1002. https://doi.org/10.1016/j.jcis.2007.08.026.

Inaba, H., Saitou, T., Tozaki, K.I., Hayashi, H., 2004. Effect of the magnetic field on the melting transition of H2O and D2O measured by a high resolution and supersensitive differential scanning calorimeter. J. Appl. Phys. 96, 6127–6132. https://doi.org/10.1063/1.1803922.

James, C., Purnell, G., James, S.J., 2015. A review of novel and innovative food freezing technologies. Food Bioprocess Technol. 8 (8), 1616–1634. https://doi.org/10.1007/s11947-015-1542-8.

Jin, S., Sun, S., Jiang, X., Zhao, Y., Wang, Y., Deng, Y., 2020. Effect of static magnetic field on the freezing process of deionized water and 0.9% NaCl solution. J. Food Process. Preserv. 44 https://doi.org/10.1111/jfpp.14663.

Kaku, M., Kamada, H., Kawata, T., Koseki, H., Abedini, S., Kojima, S., Motokawa, M., Fujita, T., Ohtani, J., Tsuka, N., Matsuda, Y., Sunagawa, H., Hernandes, R.A.M., Ohwada, N., Tanne, K., 2010. Cryopreservation of periodontal ligament cells with magnetic field for teeth banking. Cryobiology 61, 73–78. https://doi.org/10.1016/j.cryobiol.2010.05.003.

Leygonie, C., Britz, T.J., Hoffman, L.C., 2012. Impact of freezing and thawing on the quality of meat: review. Meat Sci. 91 (2), 93–98. https://doi.org/10.1016/j.meatsci.2012.01.013.

Lin, C.Y., Chang, W.J., Lee, S.Y., Feng, S.W., Lin, C.T., Fan, K.-S., Huang, H.M., 2013. Influence of a static magnetic field on the slow freezing of human erythrocytes. Int. J. Radiat. Biol. 89 (1), 51–56. https://doi.org/10.3109/09553002.2012.717731.

Lin, S.L., Chang, W.J., Lin, C.Y., Hsieh, S.C., Lee, S.Y., Fan, K.H., Lin, C.T., Huang, H.M., 2015. Static magnetic field increases survival rate of dental pulp stem cells during DMSO-free cryopreservation. Electromagn. Biol. Med. 34, 302–308. https://doi.org/10.3109/15368378.2014.919588.

Mok, J.H., Choi, W., Park, S.H., Lee, S.H., Jun, S., 2015. Emerging square wave electric field (PEF) and static magnetic field (SMF) combination technology for food freezing. Int. J. Refrig. 50, 137–145. https://doi.org/10.1016/j.ijrefrig.2014.10.025.

Orlowska, M., Havet, M., Le-Bail, A., 2009. Controlled ice nucleation under high voltage DC electrostatic field conditions. Food Res. Int. 42, 879–884. https://doi.org/10.1016/j.foodres.2009.03.015.

Otero, L., Rodríguez, A.C., Pérez-Mateos, M., Sanz, P.D., 2016. Effects of magnetic fields on freezing: application to biological products. Compr. Rev. Food Sci. Food Saf. 15, 646–667. https://doi.org/10.1111/1541-4337.12202.

Otero, L., Rodríguez, A.C., Sanz, P.D., 2018. Effects of static magnetic fields on supercooling and freezing kinetics of pure water and 0.9% NaCl solutions. J. Food Eng. 217, 34–42. https://doi.org/10.1016/j.jfoodeng.2017.08.007.

Rasmussen, A., Andersson, M., 1996. New method for determination of drip loss in pork muscles. In: Meat for the Consumer, Lillehammer, Norway, pp. 286–287.

Reddy, J.N., 2005. An Introduction to the Finite Element Method, third ed. McGraw-Hill.

Rohatgi, P.K., Jain, S.M., Adams Jr., C.M., 1974. Effect of magnetic and electrical fields on dendritic freezing of aqueous solutions of sodium chloride. Mater. Sci. Eng. 15 (2–3), 283–290.

Sanz, P.D., Elviraa, C.de, Martinob, M., Zaritzkyb, N., Otero, L., Carrascoa, J.A., 1999. Freezing rate simulation as an aid to reducing crystallization damage in foods. Meat Sci. 52 (3), 275–278. https://doi.org/10.1016/S0309-1740(99)00002-9.

Sun, W., Xu, X., Sun, W., Ying, L., Xu, C., 2007. Effect of alternated electric field on the ice formation during freezing process of 0.9% K2MnO4 water. Proceedings of the IEEE International Conference on Properties and Applications of Dielectric Materials, pp. 774–777.

Tagami, M., Hamai, M., Mogi, I., Watanabe, K., Motokawa, M., 1999. Solidification of levitating water in a gradient strong magnetic field. J. Cryst. Growth 203, 594–598. https://doi.org/10.1016/S0022-0248(99)00141-4.

Tang, J., Shao, S., Tian, C., 2019. Effects of the magnetic field on the freezing parameters of the pork. Int. J. Refrig. 107, 31–38. https://doi.org/10.1016/j.ijrefrig.2019.07.019.

Wang, Y., Zhang, B., Gong, Z., Gao, K., Ou, Y., Zhang, J., 2013. The effect of a static magnetic field on the hydrogen bonding in water using frictional experiments. J. Mol. Struct. 1052, 102–104. https://doi.org/10.1016/j.molstruc.2013.08.021, 0.

Wilson, P.W., Heneghan, A.F., Haymet, A.D.J., 2003. Ice nucleation in nature: supercooling point (SCP) measurements and the role of heterogeneous nucleation. Cryobiology 46 (1), 88–98. https://doi.org/10.1016/S0011-2240(02)00182-7.

Wei, S., Xiaobin, X., Hong, Z., Sun, W., Chuanxiang, X., 2006. The mechanism analysis of NaCl solution ice formation suppressed by electric field. In: Properties and Applications of Dielectric Materials, 2006. 8th International Conference on, pp. 770–773.

Woo, M.W., Mujumdar, A.S., 2010. Effects of electric and magnetic field on freezing and possible relevance in freeze drying. Dry. Technol. 28, 433–443. https://doi.org/10.1080/07373930903202077.

Wowk, B., 2012. Electric and magnetic fields in cryopreservation. Cryobiology 64, 301–303. https://doi.org/10.1016/j.cryobiol.2012.02.003.

Zhou, Z., Zhao, H., Han, J., 2012. Supercooling and crystallization of water under DC magnetic fields. CIE J. 63, 1405–1408.